We are IntechOpen,
the world's leading publisher of
Open Access books
Built by scientists, for scientists

4,800
Open access books available

122,000
International authors and editors

135M
Downloads

Our authors are among the

154
Countries delivered to

TOP 1%
most cited scientists

12.2%
Contributors from top 500 universities

CLARIVATE ANALYTICS

**BOOK
CITATION
INDEX**

INDEXED

WEB OF SCIENCE™

Selection of our books indexed in the Book Citation Index
in Web of Science™ Core Collection (BKCI)

Interested in publishing with us?
Contact book.department@intechopen.com

Numbers displayed above are based on latest data collected.
For more information visit www.intechopen.com

Robust Active Vibration Control of Flexible Stewart Isolators

Liu Lei, Wang Pingping, Kong Xianren and Wang Benli
School of Astronautics, Harbin Institute of Technology, Harbin 150080,
China

1. Introduction

There are increasing needs of precision pointing and extreme stability for current and future spacecrafts. The James Webb space telescope, terrestrial planet finder, space based laser, space-based interferometer and deep-space laser communication are such examples where the micro-radian pointing and nanometer level of motion stability are required by (Ford, et al, 2005), (Chen, et al, 2004) and (Winthrop, et al 2003). On the other hand, the space systems may contains many vibration sources. A satellite may contain multiple instruments; some of them may use reaction wheels, cryogenic coolers, control moment gyroscopes, solar array drives, stepper motors, and other motion devices. These devices will transmit vibrations.

Passive isolation presents a reliable, low cost solution that is effective for attenuating high frequency vibrations, but it is in general not suitable for low frequency vibration isolation, and especially, passive isolation can not provide good trade-off between resonant peak and high frequency attenuation and the trade-off between pointing command keeping and disturbance rejection. (Winthrop, et al 2003) indicates the active vibration control can overcome these limitations.

In order to achieve multi-DOF vibration isolation in broadband and precision pointing, the Stewart platform (or hexapod), especially the cubic one, has become one of the most popular approaches as in (Anderson, et al, 2000) and (Thayer, et al, 2002), as shown in Fig.1. The cubic hexapod simplifies the control topologies to allow the decoupled controller designs to be identical for each strut. In order to eliminate the micro dynamics (friction and backlash), flexure joints are generally used as in (Hanieh, 2003).

Jet Propulsion Laboratory, Air Force Research Laboratory, Naval Postgraduate School, University of Washington, Free University of Brussels, University of Wyoming, CSA Engineering Inc are very active in this research. Classic control, adaptive control, LQG control, neural control, simple robust control and other control approaches were studied by (Gawronski, et al, 2004), (Joshi, et al, 2005) and (Liu et al, 2008). In this chapter, H$_\infty$ and μ controllers are designed for the struts of Stewart platforms, suppressing the overshoot in the neighborhood of resonance frequencies. Then the dynamic model of Stewart isolator is derived, and D-K iteration is used to solve the robust controller, finally, the time domain responses to suppress disturbance are also presented.
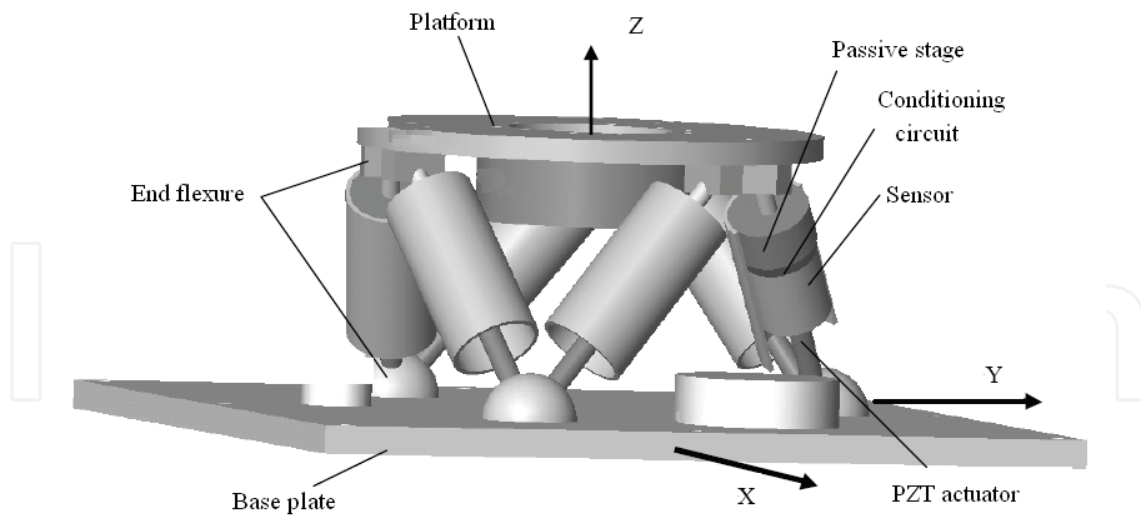
Fig. 1. Stewart platform with flexure joints

2. Dynamic model of active struts

The hexapod can be decoupled into six single-axis systems. Fig.2 shows a spring-mass model of a single strut, which can be represented as shown by equation (1-2), and the measuring output for control is the force of the strut on the side of payload. But the force due to the parasitic stiffness and damping, which represent the coupling between 6 struts, is not contained in the measuring output as in (Thayer, et al, 2002).
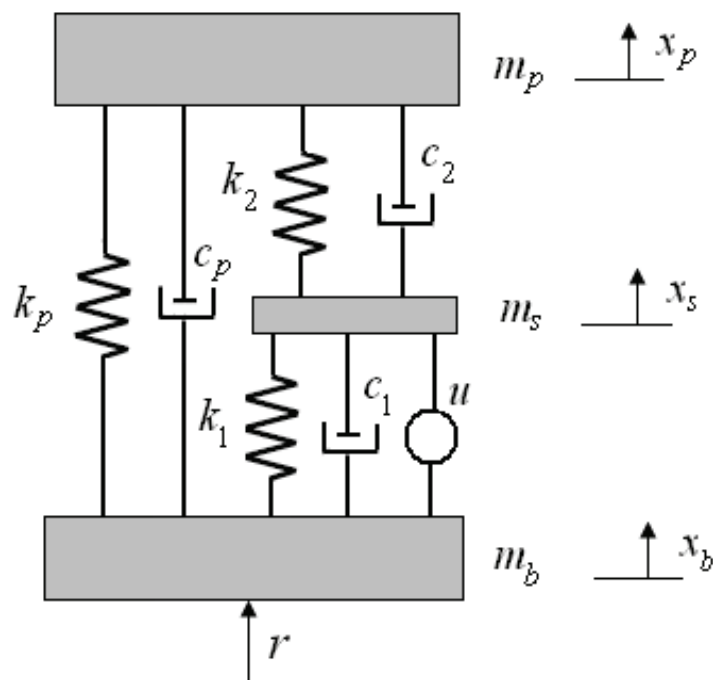

Fig. 2. Block diagram of the strut with PZT actuator

Where mass of base m_b = 200kg, mass of strut m_s = 0.254kg, Mass of payload m_p = 20kg, parasitic stiffness and damping k_p = 760N/m, c_p = 2kg/s; axis stiffness and damping of flexible joints k_2 =800000N/m, c_2 = 100kg/s; stiffness and damping of the actuator

k_1 = 80000000 N/m, c_1 = 100kg/s. u is the output of actuators, and r is the attitude control signal in addition with disturbance.

$$M\ddot{q} + D\dot{q} + Kq = f \tag{1}$$

$$y = C_q q + C_v \dot{q} \tag{2}$$

Where

$$q = (x_b, x_s, x_p)^T$$
$$M = diag([m_b, m_s, m_p])$$
$$f = \begin{pmatrix} 1 & 0 & 0 \\ 1 & -1 & 0 \end{pmatrix}^T \cdot \begin{bmatrix} r \\ u \end{bmatrix}$$
$$C_q = [0 \quad -k_2 \quad k_2]$$
$$C_v = [0 \quad -c_2 \quad c_2]$$
$$D = \begin{pmatrix} c_1 + c_p & -c_1 & -c_p \\ -c_1 & c_1 + c_2 & -c_2 \\ -c_p & -c_2 & c_p + c_2 \end{pmatrix}$$

$$K = \begin{pmatrix} k_1 + k_p & -k_1 & -k_p \\ -k_1 & k_1 + k_2 & -k_2 \\ -k_p & -k_2 & k_2 + k_p \end{pmatrix}$$

Introducing the K and M in equation $det(K - w^2 M) = 0$, the modal frequency matrix $\Omega = diag([w_1, w_2, w_3])$ is found as follows:

$$\Omega = \begin{pmatrix} 0 & 0 & 0 \\ 0 & 207.8 & 0 \\ 0 & 0 & 11670 \end{pmatrix} \tag{3}$$

Substituting Ω into $(K - \Omega^2 M)\Phi = 0$

$$\Phi = \begin{pmatrix} -0.5774 & -0.0015 & -0.0991 \\ -0.5774 & -0.9999 & -0.0777 \\ -0.5774 & 0.0003 & 0.9920 \end{pmatrix} \tag{4}$$

Introducing modal matrix Φ into equation (2), a modal equation is gotten, as shown in Equation (5). The symbols q_m, M_m, D_m and K_m are modal displacement, modal mass matrix, modal damping matrix and modal stiffness matrix.

$$\begin{cases} M_m \ddot{q}_m + D_m \dot{q}_m + K_m q_m = \Phi^T f \\ y = C_q \Phi q_m + C_v \Phi \dot{q}_m \end{cases} \tag{5}$$

Where

$$q_m = \Phi^{-1}q, D_m = \Phi^T D\Phi$$
$$M_m = \Phi^T M\Phi, K_m = \Phi^T K\Phi$$

It is seen that the first mode is a rigid mode, and the corresponding natural frequency is zero (in Ω). On the other hand, the singular value plot for the nodal model with parametric (stiffness and damping) uncertainty, as illustrated in Fig.3, a rigid mode can be found.
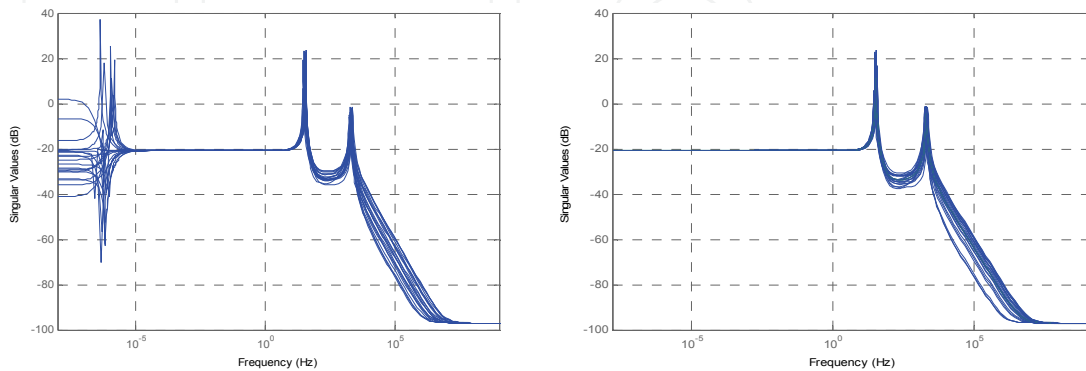

Fig. 3. Singular value plot for struts with and without rigid mode

The structures with rigid mode are unstable, but the rigid mode is the one that allows a controller to move the structures or track a command. So the rigid mode is removed when active vibration isolation controller is design. The singular value response for the dynamic model without rigid mode is shown in Fig.3, where the parametric uncertainty is also contained.

3. Robust synthesis controller design

The active vibration controller should be robust to the modeling uncertainty and parametric uncertainty, for the complex dynamic environment and model error. Robust H$_\infty$ synthesis and μ synthesis are presented in this section, and the dynamic uncertainty is contained in the model, but the parameter uncertainty is also contained in the robust stability and performance test.

3.1 performance and system interconnection

The performance objective of this chapter is based on the strict requirements of future precision spacecrafts. The low frequency pointing signals must be fully transfer through the Stewart platform, but the high frequency disturbance (both harmonic and broadband), which will disturb the precision instruments, should be isolated. So the two strict requirements are as follows:

REQ1: Low frequencies pointing command (0-5Hz)

Keep pointing attenuation within $\pm$ 0.2dB.

REQ2: Disturbance (>15Hz) and noise

Isolate the overshoot in the neighborhood of resonance frequencies 25dB, known as active damping, and isolate the noise 10dB.

The structure of closed-loop system is seen in Fig.4, *G* is the dynamic model without rigid mode, *K* is the controller to be designed, the weights describe the magnitude, relative
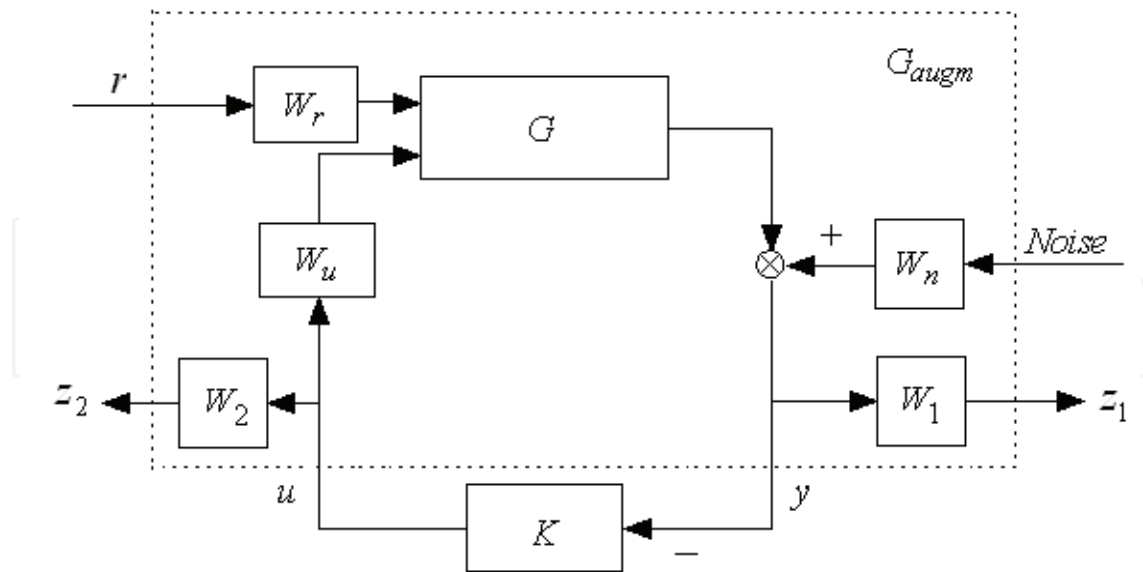
Fig. 4. Closed-loop system structure in robust design

importance and frequency content of inputs and outputs as in (Skogestad, etal, 2005). The performance weighting function W_1 reflects the relative significance of performance requirements over difference frequency ranges, because the maximum peak of G is23 dB, so the maximum of W_1 should be more than 0dB to satisfy REQ1; the control weighting function W_2 avoids saturation of the PZT actuator and suppresses the high and low frequency gains, because the maximum force of actuators is 400N, the W_2 should be more than -52dB (1/400); the noise weighting function W_n is less than 0.3N in low frequency(<300Hz), but is 1N in high frequencies(>1000Hz); W_n =10is the disturbance weighting function. The weighting functions are selected as follows:

$$W_1 = \frac{0.000445s^2 + 70s + 0.00022}{s^2 + 64.4s + 98.7}$$
$$W_2 = \frac{0.3s^2 + 154.2s + 18850}{s^2 + 62830s + 314.2} \tag{6}$$
$$W_n = \frac{s + 942.5}{s + 9425}$$

The augmented plant G_{augm} is given by equation (7):

$$\dot{x} = Ax + B_1 w + B_2 u$$
$$z = C_1 x + D_{11} w + D_{12} u \tag{7}$$
$$y = C_2 x + D_{21} w + D_{22} u$$

Where $z = [z_1, z_2]^T$, $w = r$

The PZT stacks are very precision actuators, but they are typically not highly linear, for the nonlinear factors, such as hysteresis, creep and temperature effects, and in low frequencies the error can be 10%-15% of the full scale in open loop. And so the output uncertainty of the PZT stack is represented by W_u, as seen in equation (8)

$$W_u = 1 + \frac{1}{10} \cdot \frac{2094s + 10^6}{12.6s + 10^6} \cdot \triangle \tag{8}$$

Where is $\triangle$ the complex perturbation.

3.2 Controller design

The H$_\infty$ synthesis is a mixed sensitivity H$_\infty$ suboptimal control, based on DGKF method, and μ synthesis is based on $D - K$ iteration in (Skogestad, 2005). The following criterion is used for H$_\infty$ synthesis:

$$\left\| \begin{matrix} w_1(s)S(s) \\ w_2(s)T(s) \end{matrix} \right\|_{H_\infty} < \gamma \tag{9}$$

Where $S(s)$ and $T(s)$ are the sensitivity function and complementary sensitivity function respectively.

The $D - K$ iteration μ synthesis method is based on solving the following optimization problem, for a stabilizing controller K and a diagonal constant scaling matrix D.

$$K(s) = \arg \min_{K(s) \in \kappa_S} \sup_{\omega \in \mathbb{R}} \inf_{D(s) \in D} \left\{ \bar{\sigma} \left(D(s) F_l(P,K) D^{-1}(s) \right) \right\} \tag{10}$$

Where P is the open loop interconnected transfer function matrix of the system.

The $D - K$ iteration procedure can be formulated as follows:

Step 1. Start with an initial guess for D, usually set $D = I$

Step 2. Fix D and solve the H$_\infty$ sub-optimal $K(s)$

$$K(s) = \arg \min_{K(s) \in \kappa(s)} \left\| F_l(P,K) \right\|_{H_\infty} \tag{11}$$

Step 3. Fix $K_i(s)$ and solve the convex optimal problem for D^* at each frequency over a selected frequency range.

$$D^*(j\omega) = \arg \min_{D(s) \in D} \left\{ \bar{\sigma}(\mathbf{D}(s) F_l(P,K) D^{-1}(s)) \right\} \tag{12}$$

Step 4. Curve fit $D^*(j\omega)$ to get a stable, minimum phase D^*, and compare D^* and D, stop if they closed in magnitude, otherwise go to step 2 until the tolerance is achieved.

The achieved H$_\infty$ norm γ is found to be 0.9932, and a 10th order controller is obtained. Correspondingly, the structured singular value μ is found to be 0.993, and a 12th order controller is obtained, and the bode magnitude of two controllers is in the Fig.5. During the control synthesis process, the weighting function W_1 and W_2 are adjusted repeatedly, a few trials are needed, and the final results are Equation (6).

The closed loop structure without performance weighting functions is shown in Fig.6, where G contains rigid mode.

The singular value plots for closed loops are shown in left Fig. 7, from which it can be seen that H$_\infty$ and μ controllers isolate high frequency disturbance and noise, in the neighborhood of resonance frequencies. The disturbance and noise isolated by H$_\infty$ controller is more than 27dB, and 21dB by μ controller. Right Fig. 7 shows that low frequency pointing fully transfer with attenuation less than 0.2dB. The nominal performance for H$_\infty$ synthesis controller is better than μ synthesis controller at resonance, but worse in high frequencies.
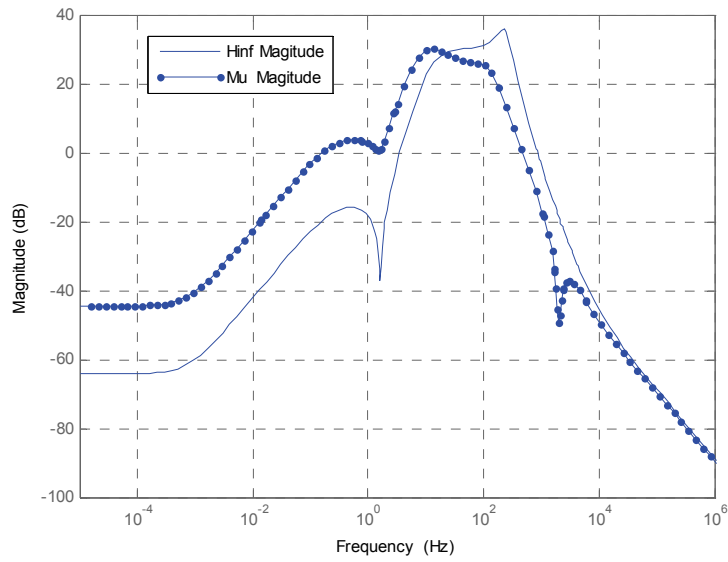
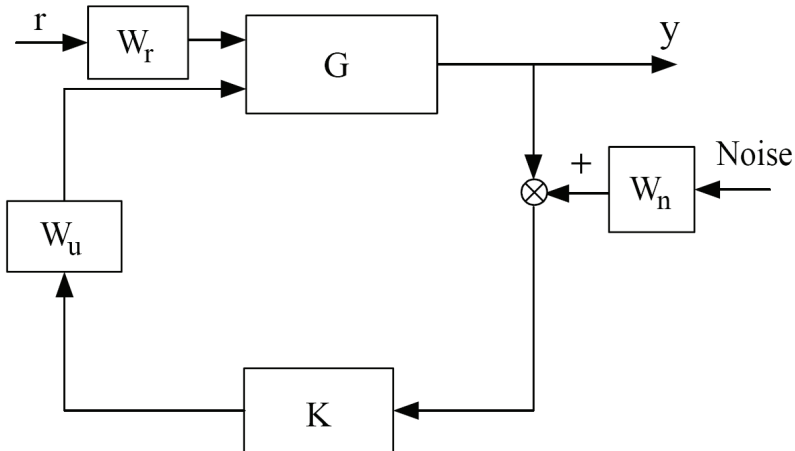Fig. 5. Bode magnitude of the controllers

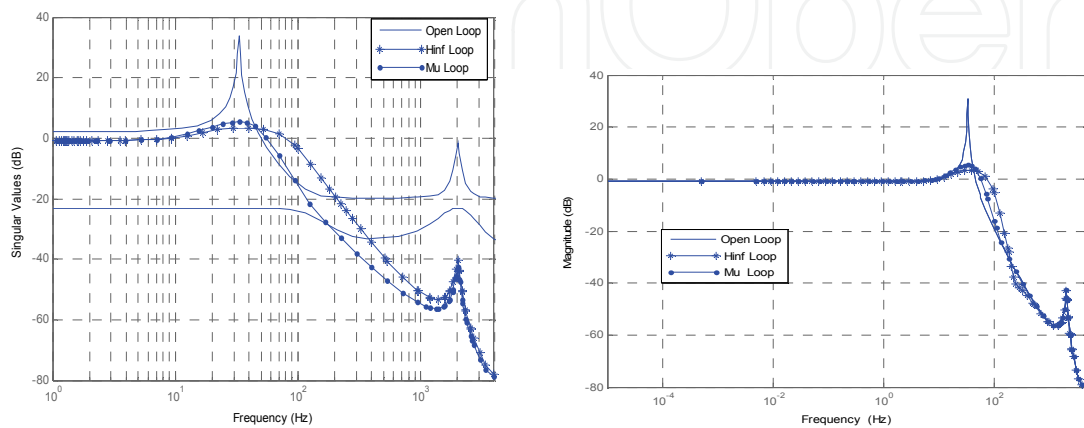Fig. 6. Closed-loop system structure for frequency responses

Fig. 7. Comparison of open loop and closed loop, Bode diagram from *r* to *y*

3.3 Robust stability analysis and controller reduction

Robust stability is very important due to various uncertainties[22] and this section will give the robust stability margins of the uncertain closed loop. By calculating, the robust stability margin for H_∞ closed loop is 1.56, and the destabilizing frequency is 625.9rad/s, and the corresponding values are 6.29 and 346rad/s for μ closed loop. Their stability robustness margins greater than 1 means that the uncertain system is stable for all values of its modeled uncertainty. On the other hand, parametric uncertainty, which is 30% change in stiffness and 80% change in damping, is considered with modeling uncertainty in order to test the robust stability and robust performance further. Fig. 8 show the singular value plots for H_∞ and μ closed loop, from which it can be seen that robust stability and robust performance for H_∞ closed loop is worse than μ closed loop in presence of large uncertainty.
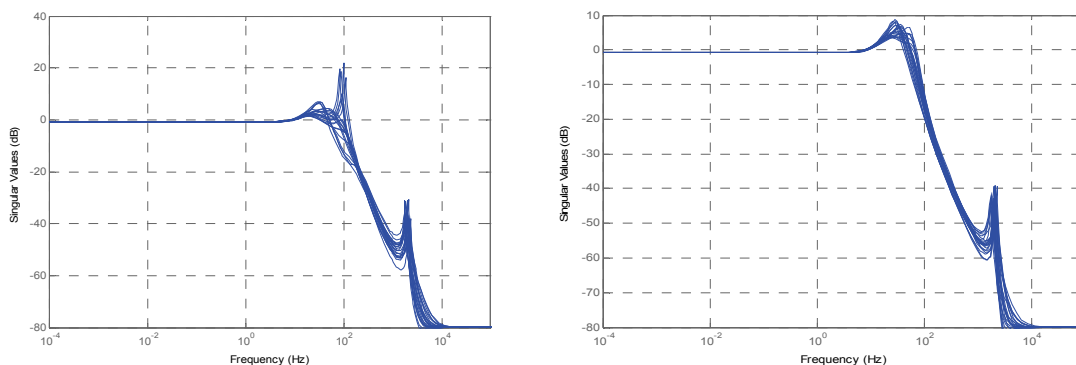
Fig. 8. Singular value plot for H_∞ closed loop and μ closed loop

As shown in section 3.2, the order of H_∞ controller is 10, and 12 of μ controller. Square root balanced model truncation, is used to reduce the order of controllers. Fig.9 shows the Bode diagrams for 6th order H_∞ controller and 8th order μ controller with their original controller.
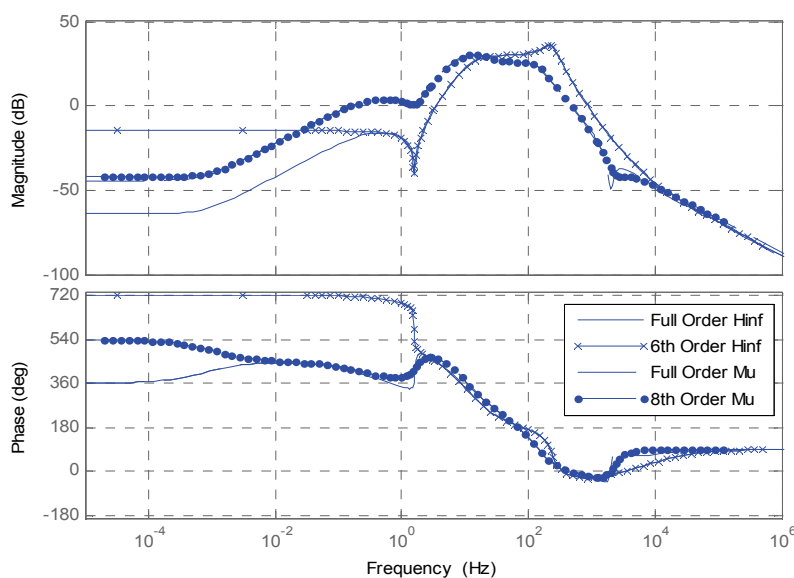

Fig. 9. Bode diagram for full and reduced controllers

The stability robustness margin is 1.56 of reduced H$_\infty$ closed loop, and 6.3 for μ closed loop, so the reduced controllers are robust stability.

4. Robust control simulations of flexible struts

The frequency responses of the open and closed loop system are shown in section 2.2 and 2.3, and this section will give the corresponding transient response for reduced order μ controller and a PI controller that is shown in Equation (13), the nominal closed loop system structure for time domain responses shown in Fig.10
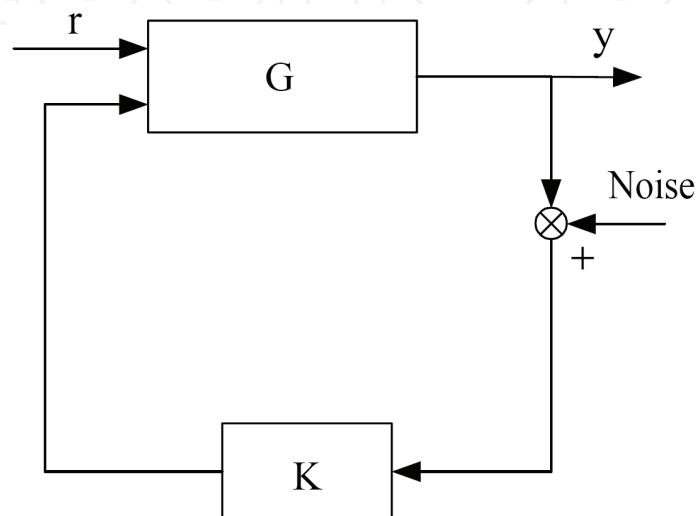
Fig. 10. Nominal closed-loop system structure

The input signal r can contain three parts: tracking signal r_0, sinusoid disturbance *dist*, and random stochastic disturbance which is Gaussian white noise with mean zero and standard deviation 0.6

$$K_{PI} = \frac{20}{s} + 32 \tag{13}$$

$$r_0 = 10\sin(t) \tag{14}$$

$$dist = 0.1\sin(33 \times 2\pi) \tag{15}$$

Figs.11 and 12 present the transient response to a harmonic disturbance input, and from the figures it can be seen that the μ controller or PI controller can effectively isolate the harmonic disturbance located at 33 Hz more than 25.2dB (94.5%).

For comparison, Fig.13 shows open response to the random disturbance, normally distributed Gaussian white noise with mean zero and standard deviation 0.60. Simultaneously, the sensor noise is also contained, which is 2% of random disturbance. Figs.14 and 15 shows the corresponding μ and PI closed loop response to the random disturbance and sensor noise. From the figures, it can be seen that the standard deviations are attenuated 11dB (70%) by μ controller, but the random disturbance is magnified to 132% by PI controller.
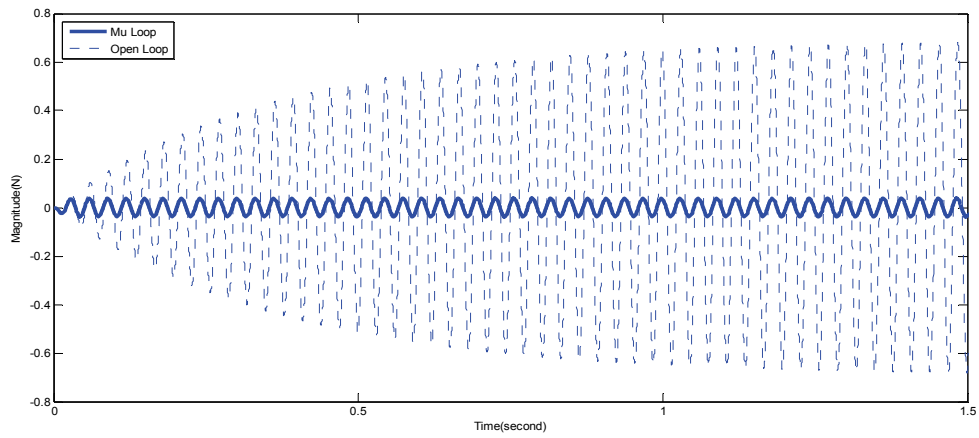
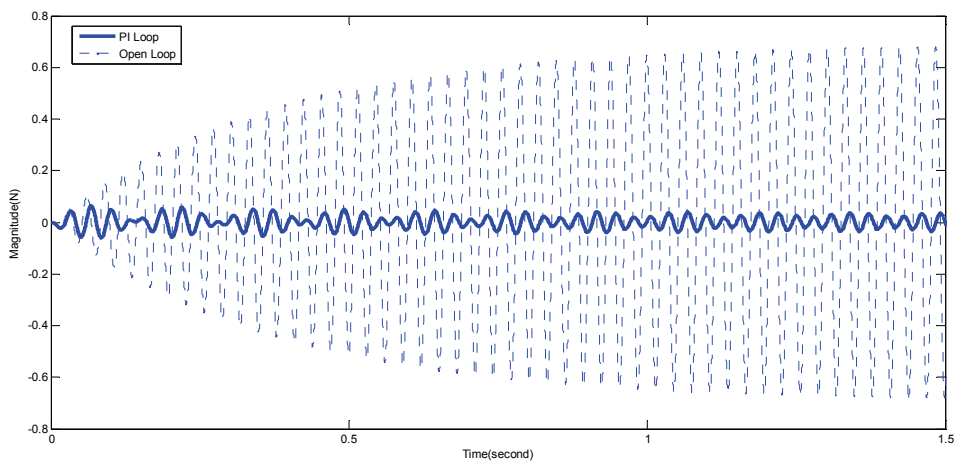Fig. 11. Open loop and μ closed loop response to sinusoid disturbance in 33 Hz

Fig. 12. Open loop and PI closed loop response to sinusoid disturbance in 33 Hz
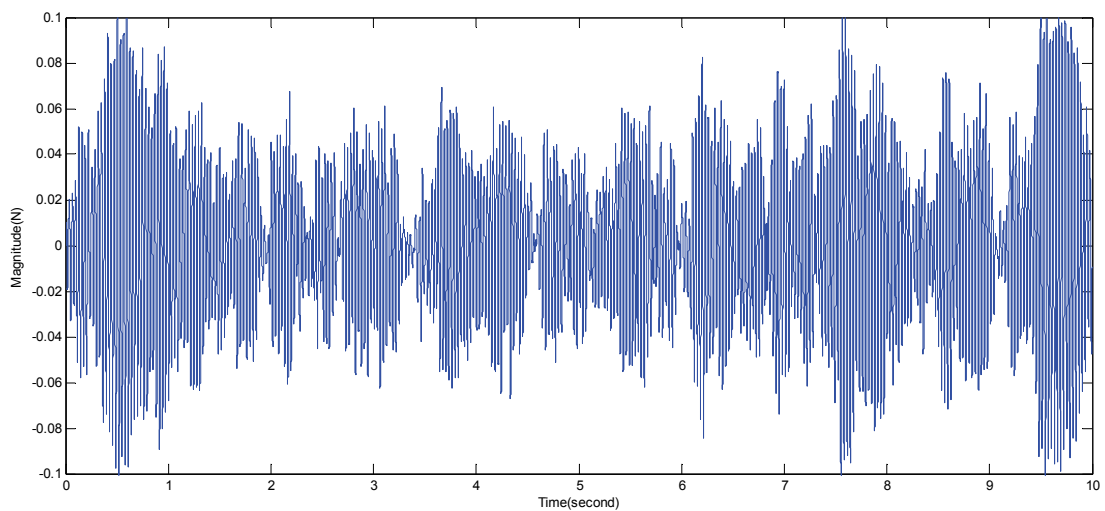

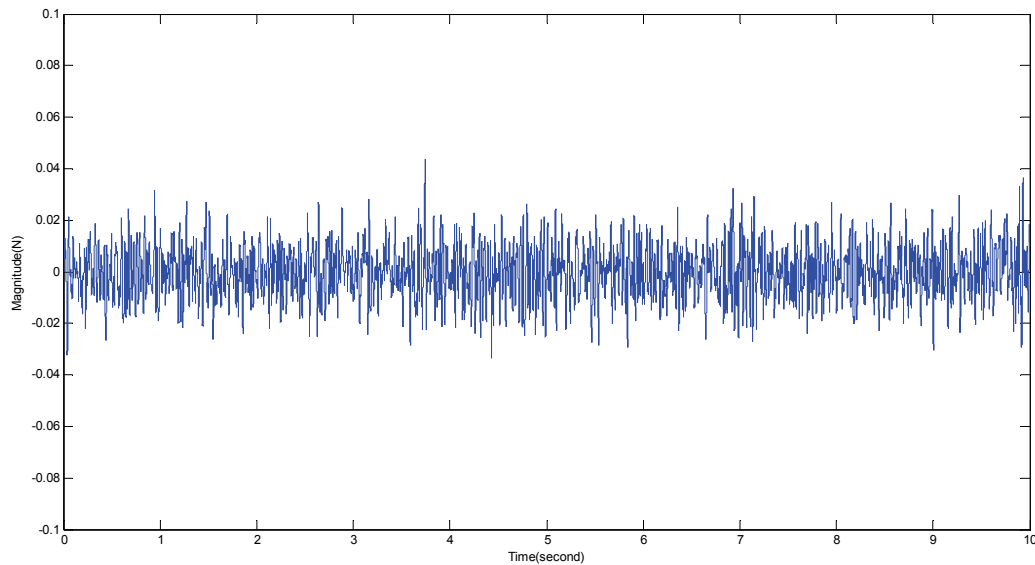Fig. 13. Open loop response to stochastic disturbance

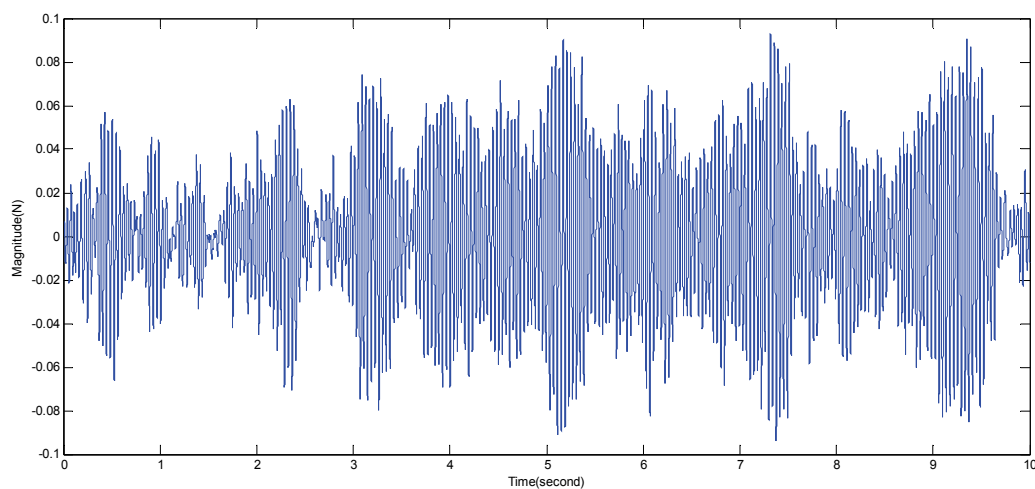Fig. 14. μ Closed loop response to stochastic disturbance

Fig. 15. PI Closed loop response to stochastic disturbance

The magnitude of PI and μ are shown in Fig.16, respectively, if the input r is a sinusoid tracking force r_0, from which it can be seen that the magnitude of PI is much lager than that of μ, and the PI maybe destroy r_0, additionally, the PZT actuators are easily saturated for the large gain.

In order to verify the two requirements of μ, another input signal is selected which is made up of tracking signal r_0, sinusoid disturbance *dist*, random disturbance and the sensor noise. The open loop response is shown in left Fig.17, from which it can be seen that the tracking signal is destroyed by the relatively small disturbance (5% of tracking signal). But the μ closed loop response, as shown in right Fig.17, gives very good result.
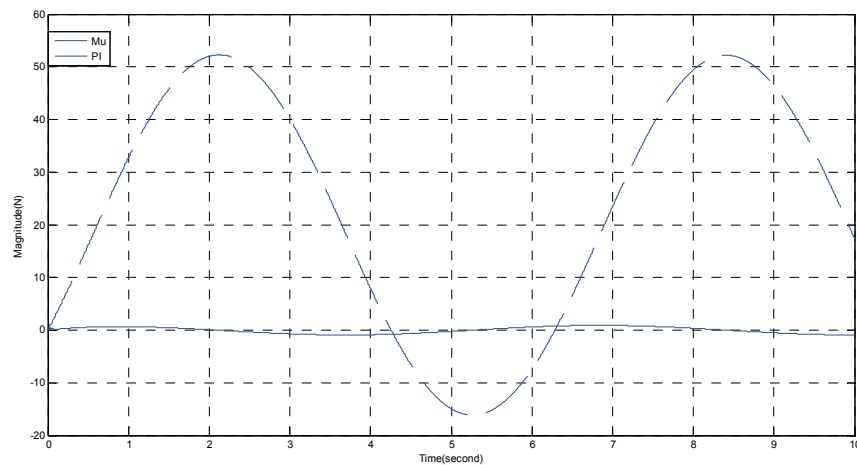
Fig. 16. The magnitude of PI and μ with input r_0
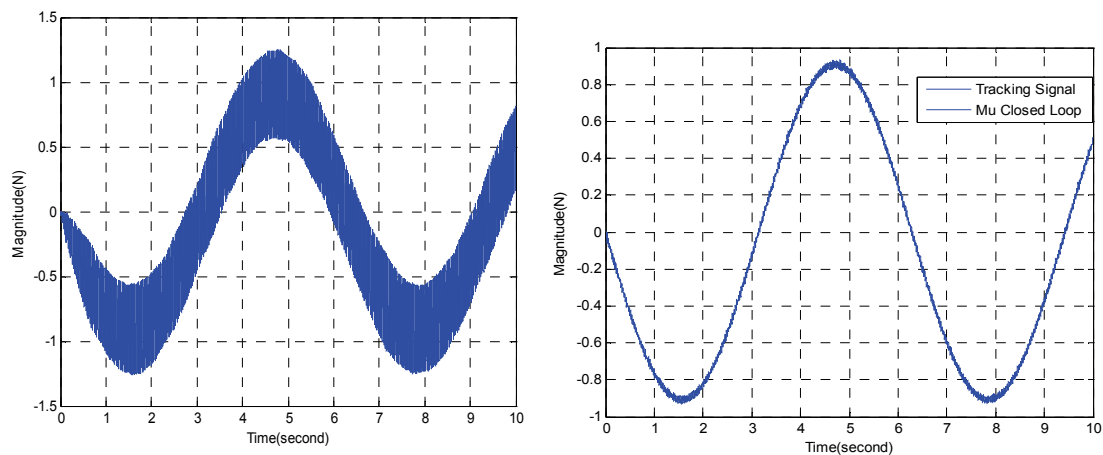

Fig. 17. Open and μ closed loop response to tracking signal with sinusoid and stochastic disturbance

5. Dynamic modeling and robust control of Stewart platforms

The Stewart isolator is used to suppress vibrations, as shown in Fig.18. It can be seen that there are 6 PZT actuators, {U}, {B}, {P} denotes the inertial frame, base frame, payload frame, respectively. A_i is the joint connecting the payload with the strut i, the mass center of the payload is $\vec{p}$ which is also the origin of the payload frame, $\vec{x}_p$ is the vector representing the origin of payload frame in the base frame.

$\vec{A}_i$ can be represented in the base frame as in equation (16)

$$\vec{A}_i = \vec{p} + \vec{x}_P \tag{16}$$

Then the inertial velocity of $\vec{A}_i$ is given in equation (17)

$$\vec{v}_i = \vec{v} + \vec{\omega} \times \vec{p}_i \tag{17}$$
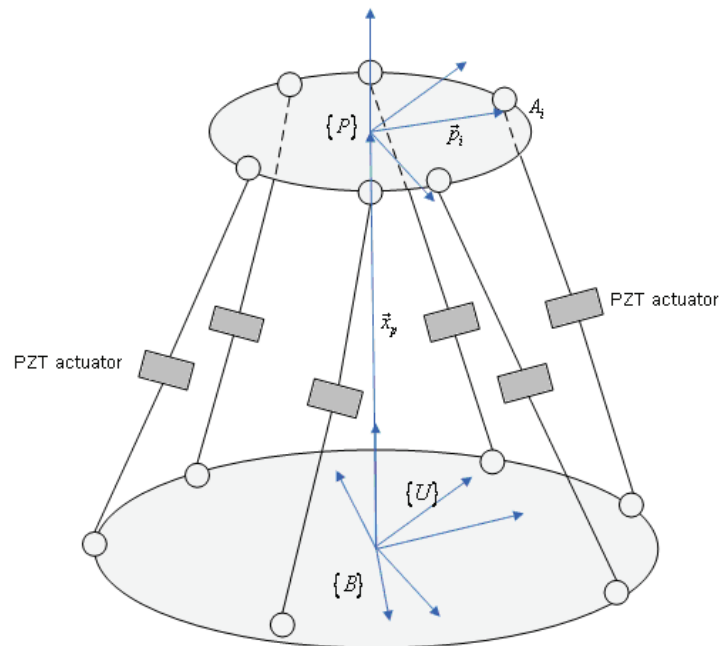
Fig. 18. Stewart isolators

The component of $\vec{v}_i$ projecting on the strut i is shown in equation

$$\dot{\vec{q}}_i = \vec{1}_i \cdot (\vec{v} + \vec{\omega} \times \vec{p}_i) \tag{18}$$

Then, it can be written in matrix form equation (19)

$$\dot{q}_i = 1_i^T v - 1_i^T p_i^* \omega \tag{19}$$

Thus, equation 19 of 6 struts can be written as equation (20)

$$\dot{q} = \begin{pmatrix} \cdots & \cdots \\ 1_i^T & -1_i^T p_i^* \\ \cdots & \cdots \end{pmatrix} \begin{pmatrix} v \\ \omega \end{pmatrix} = J\dot{\chi} \tag{20}$$

Where J is the Jacobi matrix describing the motion transformation between the struts and the payload, J can be assumed as a constant in vibration isolation.
According to Euler equation of the payload is given in equation (21)

$$r_c \times a_p m_p + J \cdot \dot{\omega} + \omega \times J \cdot \omega = T \tag{21}$$

Where r_c is the vector of the mass center of the payload in the payload frame, ω is its inertial angular velocity.
Assuming the mass center of the payload is the origin of payload frame, i.e. $r_c = 0$, Newton-Euler equation can be written as matrix equation (22)

$$\begin{bmatrix} mI_3 & 0_{3\times3} \\ 0_{3\times3} & J_{3\times3} \end{bmatrix} \ddot{\chi} + \begin{bmatrix} 0_{3\times1} \\ \omega \times J_{3\times3}\omega \end{bmatrix} = \begin{bmatrix} F \\ T \end{bmatrix} \tag{22}$$

Let $M = \begin{bmatrix} mI_3 & 0_{3 \times 3} \\ 0_{3 \times 3} & J_{3 \times 3} \end{bmatrix}$, $c(\omega) = \begin{bmatrix} 0_{3 \times 1} \\ \omega \times J_{3 \times 3}\omega \end{bmatrix}$

Then

$$M\ddot{\chi} + c(\omega) = J^T f \tag{23}$$

The dynamic model sketch can be shown in Fig. 19. Thus the equation (24) of the active struts can be obtained

$$m_s\ddot{x}_2 + (c_1 + c_2)\dot{x}_2 + (k_1 + k_2)x_2 - c_3\dot{l} - k_2 l = (c_1 + c_3)\dot{x}_1 + (k_1 + k_2)x_1 + u \tag{24}$$

$m_s = \mathrm{diag}([m_{s1}, m_{s2}, \cdots, m_{s6}])$, $l = \mathrm{diag}([l_1 \quad l_2 \quad \cdots \quad l_6])$, $k_1 = \mathrm{diag}([k_{11}, k_{21}, \cdots, k_{61}])$,
$k_2 = \mathrm{diag}([k_{12}, k_{22}, \cdots, k_{62}])$, $k_3 = \mathrm{diag}([k_{13}, k_{23}, \cdots, k_{63}])$, $c_1 = \mathrm{diag}([c_{11}, c_{21}, \cdots, c_{61}])$,
$c_2 = \mathrm{diag}([c_{12}, c_{22}, \cdots, c_{62}])$, $c_3 = \mathrm{diag}([c_{13}, c_{23}, \cdots, c_{63}])$
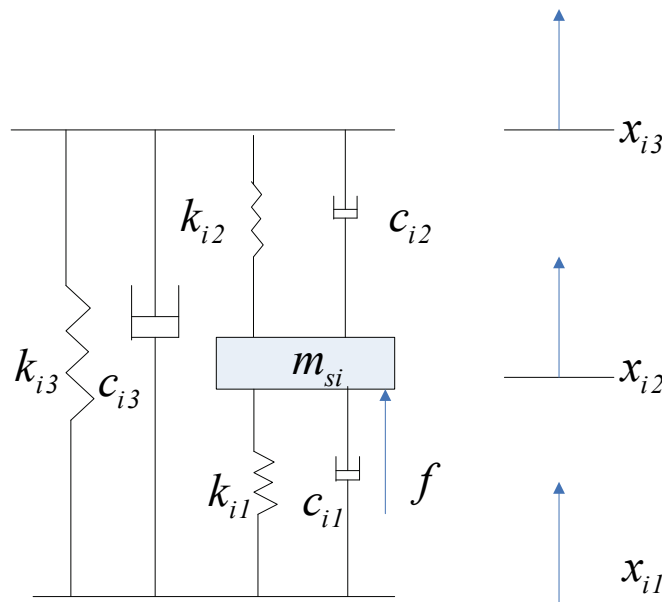

Fig. 19. The spring-mass model of struts

The force of payload subject to active struts is represented in equation (25)

$$f = -(k_2 + k_3)l - (c_2 + c_3)\dot{l} - k_2 x_1 - c_2 \dot{x}_1 \tag{25}$$

The dynamic model of the payload can be given as (26)

$$M \, {}^U J^{-1}\ddot{l} + \left(M \, {}^U_B R \dot{J}^{-1} + {}^U J^T (c_2 + c_3)\right)\dot{l} + {}^U J^{-1}(k_2 + k_3)l$$
$$= -MJ_C J_B^{-1}\ddot{x}_1 - {}^U J^T c_2 \dot{x}_1 - {}^U J^T k_2 x_1 + \left(MJ_C J_B^{-1}c_B - Mc_{BP} - c(\omega)\right) \tag{26}$$

Where $J_B = \begin{bmatrix} {}^U 1_1^T & \left({}^U_B R \, {}^B q_i \times {}^U 1_i^T\right) \\ \vdots & \vdots \\ {}^U 1_6^T & \left({}^U_B R \, {}^B q_i \times {}^U 1_i^T\right) \end{bmatrix}$, $J_C = \begin{bmatrix} I & -\left({}^U_B R^B x_P\right)^* \\ 0 & I \end{bmatrix}$

$$C_{BP} = \begin{bmatrix} 2\omega_B \times {}^U_B R \, {}^B\dot{x}_P + \omega_B \times \left(\omega_B \times {}^U_B R \, {}^B x_P \right) \\ \omega_B \times {}^U_B R \, {}^B_P \omega \end{bmatrix}$$

$$C_B = \begin{bmatrix} {}^U 1_1^T \left(\omega_B \times \left(\omega_B \times {}^U_B R \, {}^B q_1 \right) + 2\omega_B \times {}^U_B R \, {}^B \dot{q}_1 \right) \\ \vdots \\ {}^U 1_6^T \left(\omega_B \times \left(\omega_B \times {}^U_B R \, {}^B q_6 \right) + 2\omega_B \times {}^U_B R \, {}^B \dot{q}_6 \right) \end{bmatrix}$$

Assuming that the velocity $\dot{x}_2$ can be measured

$$y_v = \dot{x}_2 \tag{49}$$

Considering micro vibration in space, where disturbance force is from micro Newton to several Newton, ω_B and ${}^B_P\omega$ are small variables, such that C_B and C_{BP} can be neglected.

Using the following parameters of Stewart isolator as following;

The coordinates of 6 Joints A_i connecting strut and the payload are $[\frac{\sqrt{2}}{2} \quad -\frac{\sqrt{6}}{6} \quad \frac{\sqrt{3}}{3}]$, $[0 \quad \frac{\sqrt{6}}{3} \quad \frac{\sqrt{3}}{3}]$, $[-\frac{\sqrt{2}}{2} \quad -\frac{\sqrt{6}}{6} \quad \frac{\sqrt{3}}{3}]$ m, respectively, where two joints share the same coordinates. The corresponding base joints are $[0 \quad -\frac{\sqrt{6}}{3} \quad 0], [\frac{\sqrt{2}}{2} \quad \frac{\sqrt{6}}{6} \quad 0], [-\frac{\sqrt{2}}{2} \quad \frac{\sqrt{6}}{6} \quad 0]$ m, respectively.

The moment inertia of payload is $I = \begin{bmatrix} 20 & 2 & 2 \\ 1.5 & 2 & 1.5 \\ 1.5 & 1.5 & 2 \end{bmatrix}$ kgm²

The mass of payload $m =$15Kg, and it has uncertainty 2%. The stiffness $k_1 = 800000 I_{6\times6} N \, / \, m$, $k_2 = 800000 I_{6\times6} N \, / \, m$

Damping $c_1 = 100 I_{6\times6}$ Ns/m, $c_2 = 200 I_{6\times6}$ Ns/m, $c_3 = 10 I_{6\times6}$ Ns/m

Choosing the performance weighting function and control weighting function as following

$$W_1 = 20400 \times \frac{(s+0.2)(s+10^6)}{(s+20)(s+10^4)} I_6 \tag{50}$$

$$W_2 = 80 \times \frac{(s+1)(s+2000)}{(s+0.01)(s+20000)} I_6 \tag{51}$$

The robust controller is solved using D-K iteration, the singular values of controller can be seen in left Fig.20. The comparison of open loop (i.e. passive isolation) and closed loop with robust controller (i.e. active isolation) is shown in right Fig.20

The robust controller can suppresses vibrations from 0.3Hz to 2000Hz, and the vibrations in frequency 3Hz-800Hz is isolated more than 25dB.

6. Simulations of the robust control of Stewart isolators

Assuming Stewart isolator is excited by the disturbance force 0.1 N in 10Hz and the magnitude of x_1 is 3.93 × 10⁻⁶ m/s. The open loop response of the Stewart isolator, i.e. the passive isolation, is shown in Fig. 21. However, the closed loop response (active isolation) of Stewart isolator is shown in Fig.22. The velocity of the payload is very small, such that the second terms can be neglected, indicating the assuming of the Stewart isolator is correct.
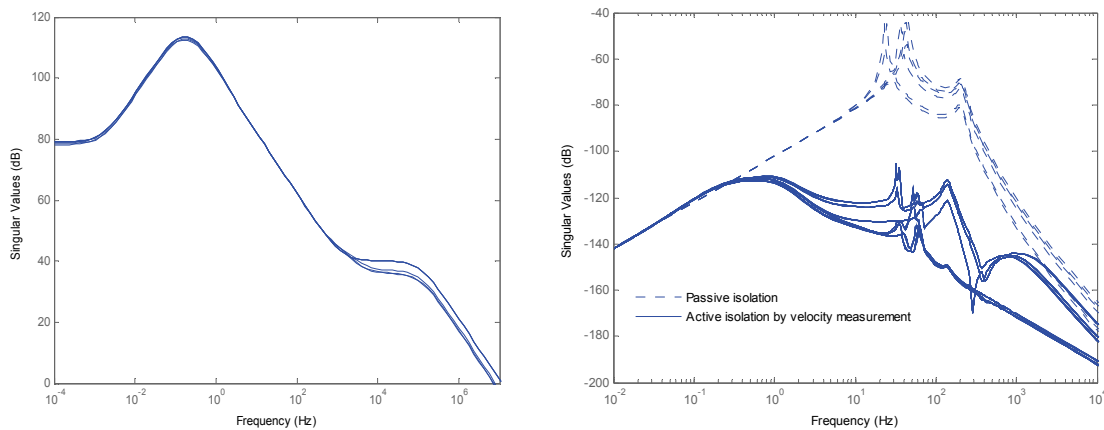
Fig. 20. The comparison of open loop and closed loop with robust controller

The maximal translation velocity of the center of payload under passive isolation is 8.8×10^{-6} (m/s), obviously, it is amplified to 124%, in other words, the Stewart isolator is a amplifier for the disturbance in 10Hz. The maximal translation velocity of the center of payload after the active isolation by robust controller is 3.4×10^{-8} (m/s), which is reduced by 99.13% (equals to 41.3dB) with respect to the input velocity, moreover, the angular velocity of the payload can be reduced by 99.13%(46.4dB) with respect to passive isolation.

Assuming the Stewart isolator is excited by white noise disturbance as shown in Fig.23, The maximal RMS velocity of input disturbance is 0.0036 (m/s), and the maximal RMS force of input disturbance is 0.1N.

With passive isolation (open loop), the RMS of the payload translation velocity is 5.74×10^{-5} (m/s), and the RMS of payload angular velocity is 3.5×10^{-3} (deg/s), indicating that the translation vibrations of the payload can be reduced by 98.4%, 35.9dB; With active isolation by robust controller, the RMS of the payload translation velocity is RMS 1.3×10^{-6} (m/s), reduced by 99.96% (68.8dB) with respect to disturbance velocity, however, the RMS of payload angular velocity is 8.4×10^{-5} (deg/s), reduced by 97.6% (32.4dB) with respect to the passive isolation.

The control signal is shown in Fig.26, the RMS of the maximal control force is 0.2N, and the maximal displacement of the PZT is less than 0.02 μm, which is far smaller than the length of the active strut.

7. Conclusions

This chapter presents multi objective robust H_∞ and μ synthesis for active vibration control of the flexure Stewart platform. The robust H_∞ and μ synthesis control of flexible struts are given considering the noise of sensors. The simulation indicates that the reduced controllers, by square root balanced model truncation, can keep the robust stability compared with the original controllers. Finally, dynamic model and robust control of Stewart isolators is given, and the robust controller can reduce vibrations in 3Hz-800Hz more than 96%.

8. References

Anderson H.; Fumo P, Ervin S. (2000). Satellite ultra-quiet isolation technology experiment (SUITE), *proceeding of IEEE aerospace conference* 4: 219-313

Chen J., Hospodar E, & Agrawal B. (2004). Development of a hexapod laser-based metrology system for finer optical beam pointing control, *AIAI Paper*, 2004-3146

Ford V. (2005). Terrestrial planet finder coronagraph observatory summary, *NASA report* document ID: 20060043653

Gawronski K. (2004). *Advanced structural dynamics and active control of structures*, New York: Springer

Gu D-W., Petkov P., Konstantinov M. (2005). *Robust control design with MATLAB*, London: SpringerVerlag

Hanieh A. (2003). *Active isolation and damping of vibration via Stewart platform*, PhD thesis, Free University of Brussels

Joshi A, Kim W. (2005). Modeling and multivariable control design methodologies for hexapod-based satellite vibration isolation, *Journal of Dynamic Systems*, Measurement, and Control, 127(4): 700-704

Liu L, Wang B. (2008). Multi objective robust active vibration control for flexure iointed struts of Stewart platforms via H$_\infty$ and μ Synthesis, *Chinese Journal of Aeronautics*, 21(2): 125-133

M. McMickell, T. Kreider, E. Hansen, et al, (2007). Optical Payload Isolation using the Miniature Vibration Isolation System (MVIS-II), *In Proc. of SPIE Vol.6527, Industrial and Commercial Applications of Smart Structures Technologies*, No.652703

Skogestad S, Postlethwaite I. (2005). *Multivariable feedback control: design and analysis,* 2nd edition, Chichester: John Wiley & Sons Ltd

Thayer D, Campbell C. (2002). Six-axis vibration isolation system using soft actuators and multiple sensors, *Journal of Spacecraft and Rockets*, 39(2):206-212

Winthrop M, Cobb R. (2003). Survey of state of the art vibration isolation research and technology for space applications, *proceeding of SPIE on 2003 Smart Structures and Materials*, 5052:13-26
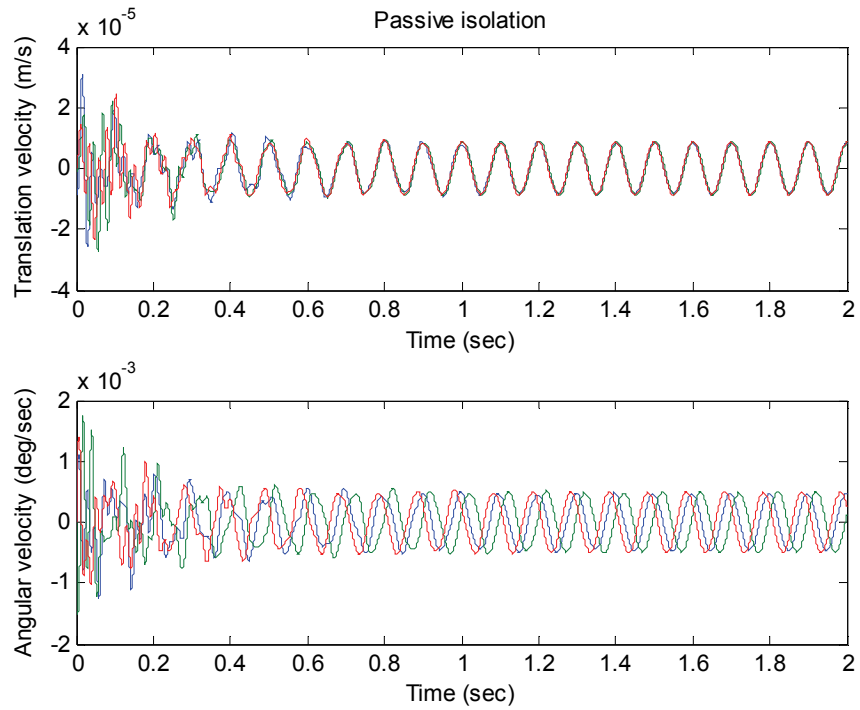
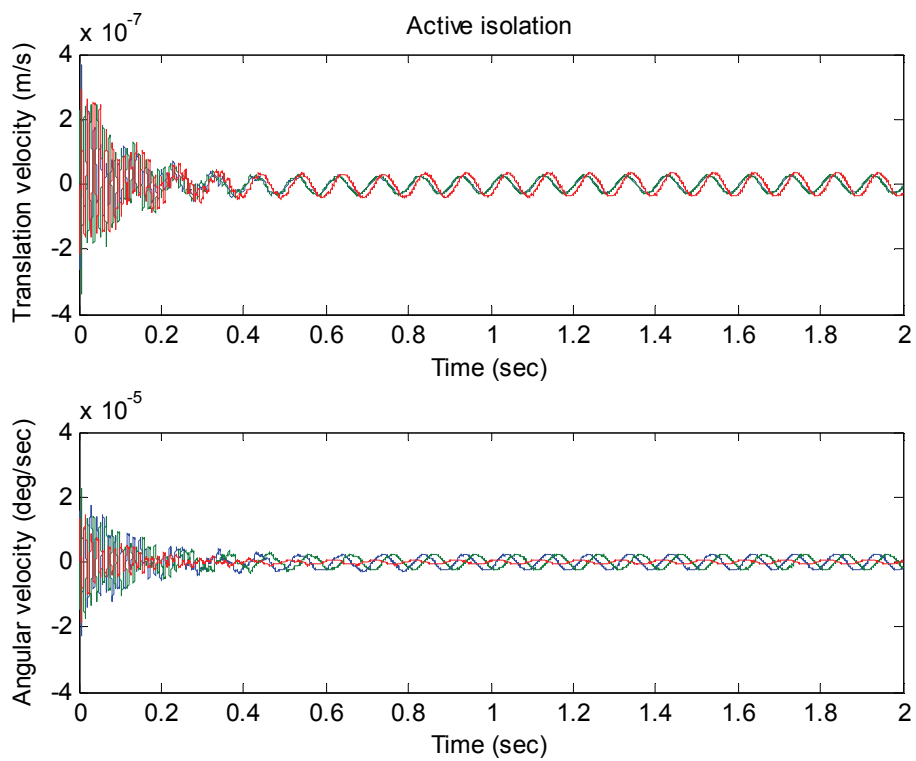Fig. 21. the velocity of the payload under passive isolation(open loop)

Fig. 22. The velocity of the payload under active isolation(close loop)
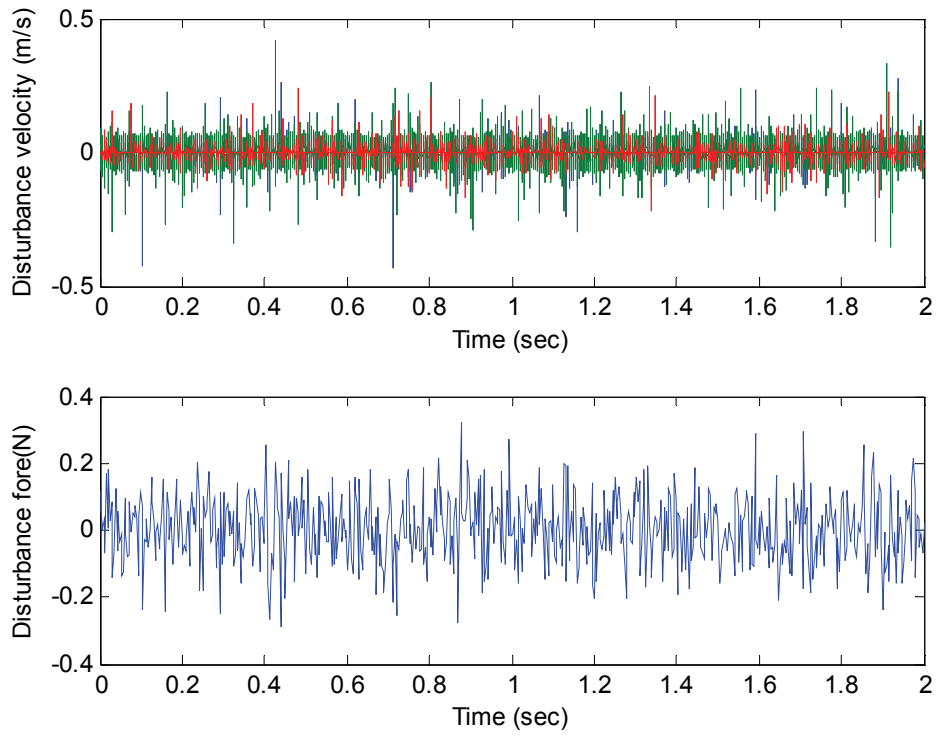
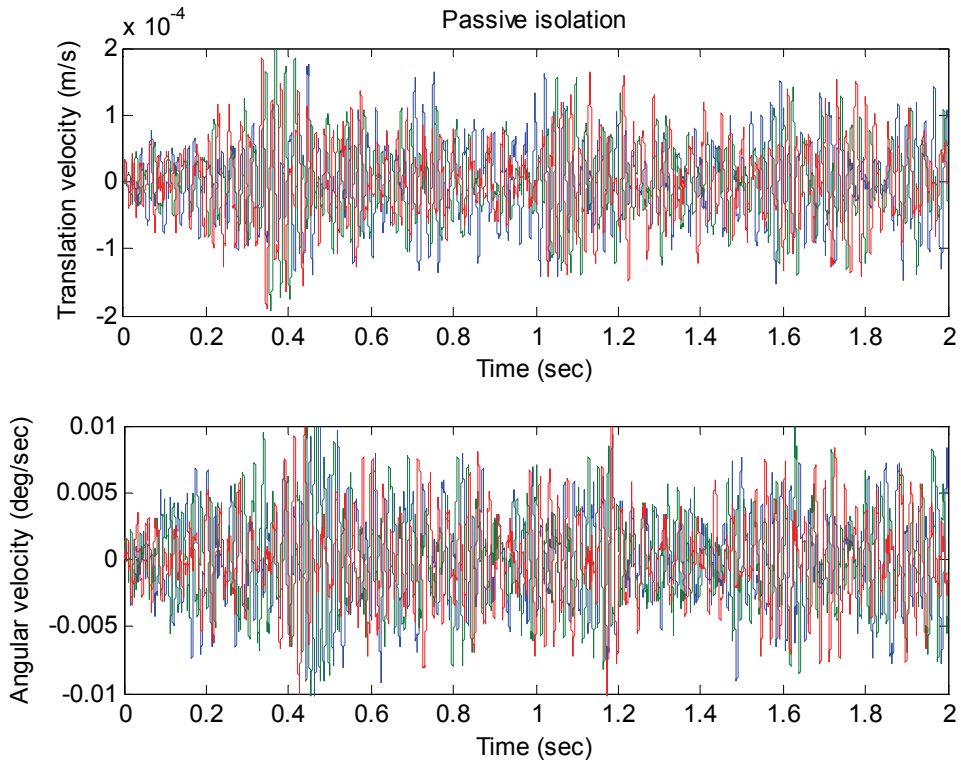Fig. 23. The velocity and force of disturbance of Stewart isolator

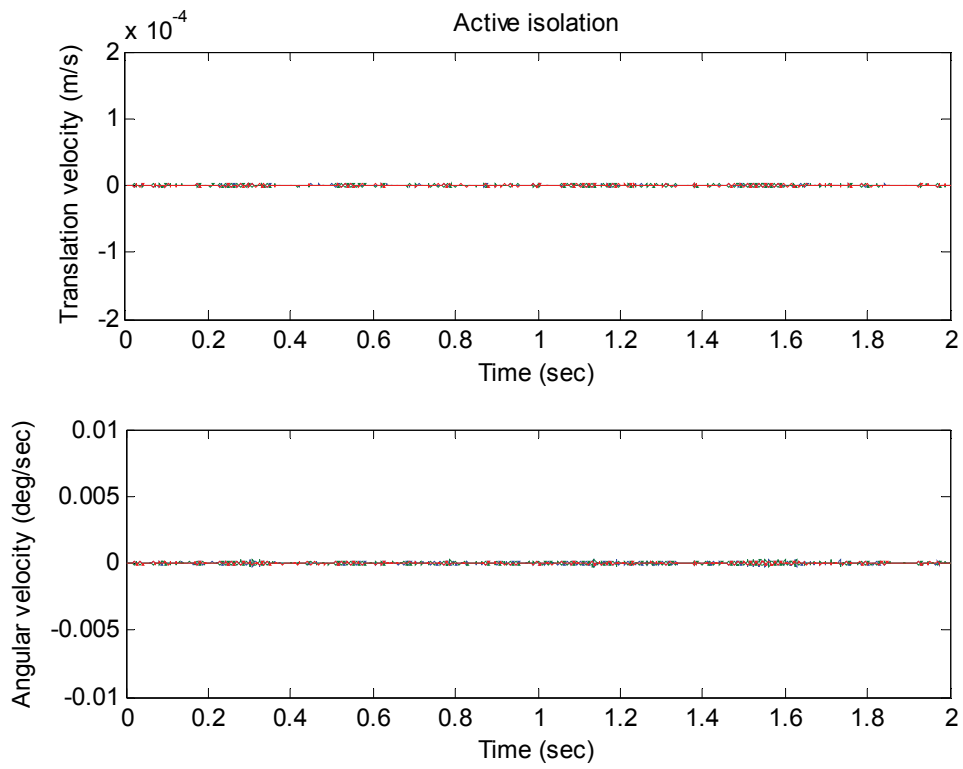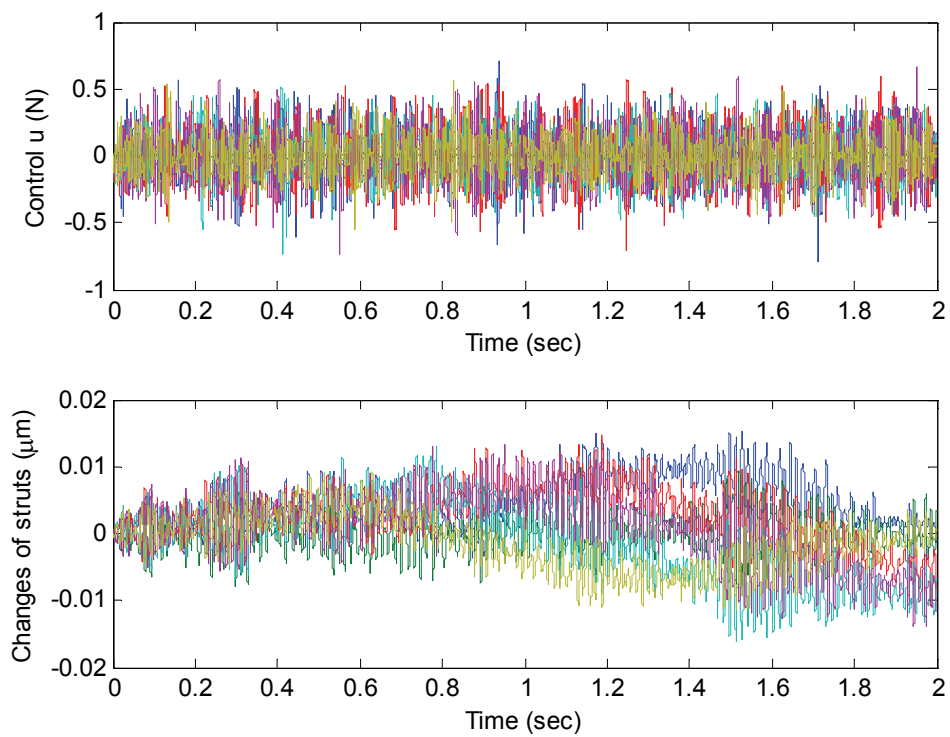Fig. 24. The velocity of the payload under passive isolation(open loop)

Fig. 25. The velocity of the payload under active isolation (close loop)

Fig. 26. The control signal and variances of 6 struts

Vibration Control

Edited by Mickaël Lallart

Vibrations are a part of our environment and daily life. Many of them are useful and are needed for many purposes, one of the best example being the hearing system. Nevertheless, vibrations are often undesirable and have to be suppressed or reduced, as they may be harmful to structures by generating damages or compromise the comfort of users through noise generation of mechanical wave transmission to the body. the purpose of this book is to present basic and advanced methods for efficiently controlling the vibrations and limiting their effects. Open-access publishing is an extraordinary opportunity for a wide dissemination of high quality research. This book is not an exception to this, and I am proud to introduce the works performed by experts from all over the world.

How to reference

In order to correctly reference this scholarly work, feel free to copy and paste the following:

Lei Liu, Pingping Wang, Xianren Kong and Benli Wang (2010). Robust Active Vibration Control of Flexible Stewart Isolators, Vibration Control, Mickaël Lallart (Ed.), ISBN: 978-953-307-117-6, InTech, Available from: http://www.intechopen.com/books/vibration-control/robust-active-vibration-control-of-flexible-stewart-isolators

INTECH

open science | open minds